*Progress In Electromagnetics Research M, Vol. 73, 71–79, 2018*

# Electromagnetic Wave Reflectance, Transmittance, and Absorption in a Graphene-Covered Uniaxial Crystal Slab

**Muhammad Azam[1], Irfan Toqeer[1], Abdul Ghaffar[1, *], Muhammad Y. Naz[1], Majeed A. S. Alkanhal[2], and Yasin Khan[2]**

**Abstract**—A theoretical investigation of the interaction of electromagnetic plane waves with a uniaxial crystal slab bounded by two graphene layers from both sides placed in free space is presented in this paper. An $8\times8$ matrix method is developed using boundary conditions at a grapheneuniaxial anisotropic crystal interface and a uniaxial anisotropic crystal-graphene interface. The developed matrix is used to find reflection and transmission coefficients by Crammer's rule. Numerical results are presented to demonstrate the effect of frequency of the incident wave, thickness of the uniaxial crystal slab, and Fermi energy of the graphene on the reflected and transmitted energies. The presented formulations and results are confirmed by published results of some limited cases.

## 1. INTRODUCTION

Material technology is progressing with great pace towards constructing new materials with specific electromagnetic (EM) and optical properties which do not exist in natural materials. One of the frontiers at which major conquests are being made is that of new materials like graphene. In recent years, graphene has attained a lot of attention in terms of theoretical analysis of electrodynamic and optical characterization [1–4]. Graphene is a monolayer of carbon atoms with mass-less linear electron/hole dispersion with the effective velocity of light [5]. The special spectrum of the charge carriers leads to a number of interesting transport properties, which have been intensively studied in the literature [6, 7]. Graphene has potential applications in optoelectronics [8–13]. It has renowned applications in the development of bioelectric sensory devices to measure glucose levels, hemoglobin levels, and cholesterol due to its high conductivity [14].

In metamaterial engineering, micro-sized devices have been theorized and realized for the manipulation of Terahertz frequency range. It is noticed from literature that graphene based structures can make more compact devices in the range of nano-scale, to manipulate and control the terahertz frequencies which can bring more advancement in metamaterial engineering [5, 15–17]. Tunable THz metamaterials are flexible in terms of their properties which can be varied through different influences. Graphene possesses a number of unique and extraordinary properties, such as high charge carrier mobility, electronic energy spectrum without a gap between the conduction and valence bands, and frequency dependent absorption of electromagnetic radiation. Several researches have been carried out on electromagnetic radiation interaction with graphene [18–20]. These studies show that both TE and TM polarized plasmons can exist in graphene [5, 15–17]. The reflection and transmission of electromagnetic waves by a graphene layer and graphene super lattice have been investigated [21, 22]. Othman et al. [23] studied the tuneability characteristics at THz frequencies of graphene-dielectric multilayer.

*Received 4 June 2018, Accepted 24 August 2018, Scheduled 7 September 2018*

* Corresponding author: Ch. Abdul Ghaffar (chabdulghaffar@yahoo.com).

[1] Department of Physics, University of Agriculture, Faisalabad, Pakistan. [2] Department of Electrical Engineering, King Saud University, Saudi Arabia.

It is observed from literature survey that graphene coatings on different metamaterials (uniaxial crystal) may route to promise for development of different nano-devices and hybrid optical elements including modulators, biochemical sensors and polarizers [24, 25]. Interaction of electromagnetic waves with a planar uniaxial crystal interface [26] is of great interest and practical importance because this consideration is expected to play a role in the development of diagnostic tools for remote sensing, in the design of electromagnetic shields, and in the inspection of structural deformation. However, the impact of graphene on uniaxial crystal slab has not been addressed yet. In this paper we introduce a concept for manipulating the interaction of electromagnetic wave at a graphene-uniaxial anisotropic crystal interface and uniaxial anisotropic crystal-graphene interface. We derive a matrix which connects the incident, reflected and transmitted fields to obtain the reflection and the transmission coefficients by Crammer's rule in matrix form. The numerical computations have been carried out to calculate the reflectance, transmittance, and absorption of electromagnetic energy at different values of Fermi energy of graphene, frequencies of the incoming wave, and slab thicknesses. The time-harmonic ($i\omega t$) dependence is adopted and suppressed in what follows.

## 2. FORMULATIONS

Consider a uniaxial crystal slab of thickness $d$ bounded by two graphene layers from both sides placed in free space as shown in Figure 1.

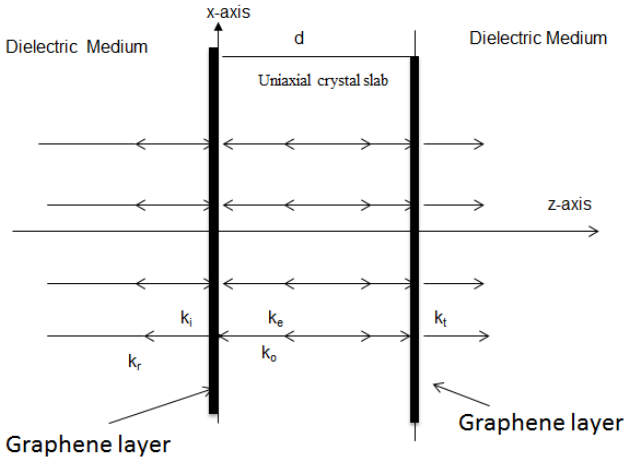


**Figure 1.** Geometry of a graphene covered uniaxial crystal slab.

Constitutive relations for the uniaxial anisotropic medium are expressed as [26]

$$\mathbf{D} = \overline{\overline{\varepsilon}} \cdot \mathbf{E} \tag{1}$$

$$\mathbf{B} = \mu \mathbf{H} \tag{2}$$

The permittivity tensor of the uniaxial crystal can be described as follows

$$\overline{\overline{\varepsilon}} = \begin{vmatrix} \varepsilon_t & 0 & 0 \\ 0 & \varepsilon_t & 0 \\ 0 & 0 & \varepsilon_z \end{vmatrix} \tag{3}$$

where $\varepsilon_t$ is the permittivity of the uniaxial crystal perpendicular to the optical axis, and $\varepsilon_z$ is the permittivity along the optical axis of the uniaxial crystal under consideration. The free space permeability and permittivity parameters are $\mu_0$ and $\varepsilon_0$, respectively. Two propagation modes exist inside the uniaxial crystal; one with ordinary wave number $k_o = \omega\sqrt{\mu_0\varepsilon_t}$ and the other with extraordinary wave number $k_e = k_0\sqrt{\frac{\varepsilon_z}{\varepsilon_t+\gamma^2(\varepsilon_z-\varepsilon_t)}}$, where $\gamma$ is the direction cosine with respect to the $z$-axis. The appropriate form to express the fields in the zone $z \leq 0$ is represented by the follows:

$$\mathbf{E_{0i}} = E_i \hat{e}_x \exp(jk_i z) \tag{4}$$

$$\mathbf{H_{0i}} = \frac{k_i}{\omega\mu} E_i \hat{e}_y \exp(jk_i z) \tag{5}$$

where $k_i = \omega\sqrt{\mu_0\varepsilon_0}$. The reflected electric and magnetic fields are

$$\mathbf{E_r} = \left(E_{r\parallel}\hat{e}_x + E_{r\perp}\hat{e}_y\right)\exp(-jk_i z) \tag{6}$$

$$\mathbf{H_r} = \frac{k_i}{\omega\mu}\left(E_{r\perp}\hat{e}_x - E_{r\parallel}\hat{e}_y\right)\exp(-jk_i z) \tag{7}$$

The waves propagating into the uniaxial crystal slab, as ordinary and extraordinary waves, can be written as

$$\begin{aligned}\mathbf{E}^u &= \left(E_{o1}e^{jk_o z} + E_{o2}e^{-jk_o z}\right)(\hat{e}_x\cos\varphi + \sin\varphi\hat{e}_y) \\ &\quad + \left(E_{e1}e^{jk_e z} + E_{e2}e^{-jk_e z}\right)(\hat{e}_x\sin\varphi\cos\delta - \cos\varphi\cos\delta\hat{e}_y) \end{aligned}\tag{8}$$

$$\begin{aligned}\mathbf{H}^u &= \frac{k_o}{\omega\mu}\left(E_{o1}e^{jk_o z} + E_{o2}e^{-jk_o z}\right)(\hat{e}_y\sin\varphi - \hat{e}_x\cos\varphi) \\ &\quad - \frac{k_e}{\omega\mu}\left(E_{e1}e^{jk_e z} + E_{e2}e^{-jk_e z}\right)(\hat{e}_x\sin\varphi\cos\delta + \hat{e}_y\cos\varphi\cos\delta) \end{aligned}\tag{9}$$

where $\varphi$ is the angle between the incident polarization and its normal.

The transmitted field out of the uniaxial crystal slab is represent by

$$\mathbf{E_t} = \left(E_{t\parallel}\hat{e}_x + E_{t\perp}\hat{e}_y\right)\exp(jk_t(z-d)) \tag{10}$$

$$\mathbf{H_t} = \frac{k_t}{\omega\mu}\left(E_{t\parallel}\hat{e}_y - E_{t\perp}\hat{e}_x\right)\exp(jk_t(z-d)) \tag{11}$$

Applying the boundary conditions at $z = 0$

$$(\mathbf{E_i} + \mathbf{E_r}) \times \hat{e}_z = \mathbf{E}^u \times \hat{e}_z \tag{12}$$

$$(\mathbf{H_i} + \mathbf{H_r}) \times \hat{e}_z = \mathbf{H}^u \times \hat{e}_z + 4\pi\mathbf{J}/c \tag{13}$$

With the boundary conditions at $z = d$ given by

$$\mathbf{E}^u \times \hat{e}_z = \mathbf{E_t} \times \hat{e}_z \tag{14}$$

$$\mathbf{H}^u \times \hat{e}_z + 4\pi\mathbf{J}/c = \mathbf{H_t} \times \hat{e}_z \tag{15}$$

Utilizing the continuity equation in momentum space given as [18]

$$\rho = j_x(\omega)k_x/\omega \tag{16}$$

and Ohm's law for the current component is written as

$$J_x(\omega) = \sigma(\omega)E_{o,e}^{1,2} = \sigma_g(\omega)E_{o,e}^{1,2} \tag{17}$$

where $\sigma_g$ is the graphene conductivity and defined as

$$\sigma_g = \sigma_1' + j\sigma_1'' + \sigma_D \tag{18}$$

where $\sigma_1' = \sigma_0(1 + \frac{1}{\pi}\tan^{-1}\frac{\hbar\omega - 2E_F}{\hbar\Gamma} - \frac{1}{\pi}\tan^{-1}\frac{\hbar\omega + 2E_F}{\hbar\Gamma} -)$, $\sigma_1'' = \sigma_0\frac{1}{\pi}\ln\frac{(2E_F+\hbar\omega)^2+\hbar^2\Gamma^2}{(2E_F-\hbar\omega)^2+\hbar^2\Gamma^2}$, and $\sigma_D = \sigma_0\frac{4E_F}{\pi}\ln\frac{1}{\hbar\Gamma - j\hbar\omega}$.

In graphene, $\sigma_0 = \frac{\pi e^2}{2\hbar}$ is the universal conductivity, $\Gamma$ the inverse of the momentum relaxation time, and $E_F > 0$ the Fermi level position with respect to the Dirac point. We solve the above equations in sequence to seek the complete solutions which will lead to inspecting the magnitude of the respective field components in the following forms.

$$\begin{bmatrix} E_{r\parallel} \\ E_{r\perp} \\ E_{o1} \\ E_{o2} \\ E_{e1} \\ E_{e2} \\ E_{t\parallel} \\ E_{t\perp} \end{bmatrix} = A^{-1}\begin{bmatrix} E_{i\parallel} \\ 0 \\ k_i E_{i\parallel} \\ 0 \\ 0 \\ 0 \\ k_i E_{i\parallel} \\ k_i E_{i\perp} \end{bmatrix} \tag{19}$$

where

$$A=\begin{bmatrix} -1 & 0 & \cos\varphi & \cos\varphi & \sin\varphi\cos\delta & \sin\varphi\cos\delta & 0 & 0 \\ 0 & -1 & \sin\varphi & \sin\varphi & \cos\varphi\cos\delta & -\cos\varphi\cos\delta & 0 & 0 \\ k_i & 0 & \cos\varphi\left(k_o+\frac{4\pi\sigma_g}{c}\right) & -\cos\varphi\left(k_o+\frac{4\pi\sigma_g}{c}\right) & \sin\varphi\cos\delta\left(k_e+\frac{4\pi\sigma_g}{c}\right) & -\sin\varphi\cos\delta\left(k_e+\frac{4\pi\sigma_g}{c}\right) & 0 & 0 \\ 0 & k_i & k_o\sin\varphi & -k_o\sin\varphi & \sin\varphi\cos\delta & -\sin\varphi\cos\delta & 0 & 0 \\ 0 & 0 & \cos\varphi e^{jk_od} & \cos\varphi e^{-jk_od} & \sin\varphi\sin\delta e^{jk_ed} & \sin\varphi\sin\delta e^{-jk_ed} & 0 & -1 \\ 0 & 0 & \cos\varphi e^{jk_od} & \cos\varphi e^{-jk_od} & \sin\varphi\sin\delta e^{jk_ed} & \sin\varphi\sin\delta e^{-jk_ed} & -1 & 0 \\ 0 & 0 & \cos\varphi(k_o+\frac{4\pi\sigma_g}{c})e^{jk_od} & -\cos\varphi\,(k_o+\frac{4\pi\sigma_g}{c})\,e^{-jk_od} & \sin\varphi\cos\delta\,(k_e+\frac{4\pi\sigma_g}{c})\,e^{jk_ed} & -\sin\varphi\cos\delta\,(k_e+\frac{4\pi\sigma_g}{c})\,e^{-jk_ed} & 0 & -k_i \\ 0 & 0 & k_o\sin\varphi\cos\delta e^{jk_od} & -k_o\sin\varphi\cos\delta e^{-jk_od} & k_e\sin\varphi\cos\delta e^{jk_ed} & -k_e\sin\varphi\cos\delta e^{-jk_ed} & k_i & 0 \end{bmatrix}.$$

The above system of eight nonhomogeneous equations in $8\times 8$ matrix form is used to calculate the refection and transmission coefficients of the uniaxial crystal slab covered by graphene which can be found numerically by using Crammer's rule. The reflected power, transmitted power and absorption power can be found by the following formulas

$$P_r = \left|E_{r\|}\right|^2 + \left|E_{r\perp}\right|^2 \tag{20}$$

$$P_t = \left|E_{t\|}\right|^2 + \left|E_{t\perp}\right|^2 \tag{21}$$

$$A = 1 - P_r - P_t \tag{22}$$

## 3. NUMERICAL RESULTS AND DISCUSSION

In this section, the above-described procedure is applied to compute the values of the reflection coefficients and the transmission coefficients at the interfaces. Consequently, the reflected power, transmitted power, and absorbed power by the uniaxial crystal plate covered by the graphene layers, when it is excited by an electromagnetic plane wave from free space, are acquired. If we let $\sigma_g = 0$, the resulting reflected power, transmitted power, and absorbed power exactly match with reflected power, transmitted power, and absorbed power obtained using Equations (33) and (37) of Lenker [26] by replacing $E_{r\|} = r$, $E_{r\perp} = r'$, $E_{t\|} = t$ and $E_{t\perp} = t'$ as depicted in Figure 2. Figure 2 shows comparison of reflected power, transmitted power and absorption power for our case (solid line) and of Lenker [26] (dashed line) at $\varphi = 45°$, $\delta = 45°$, $d = 10$, $\Gamma = 2.6\,\text{meV}$, $\varepsilon_t = 4\varepsilon_0$, $\varepsilon_z = 3\varepsilon_0$, and $\gamma = 0.96$. If $\varphi = 0$, $\varepsilon_t = \varepsilon_z = \varepsilon_2$, $\varepsilon_0 = \varepsilon_1$, the resulting expressions can approach the transmissivity and reflectivity of two

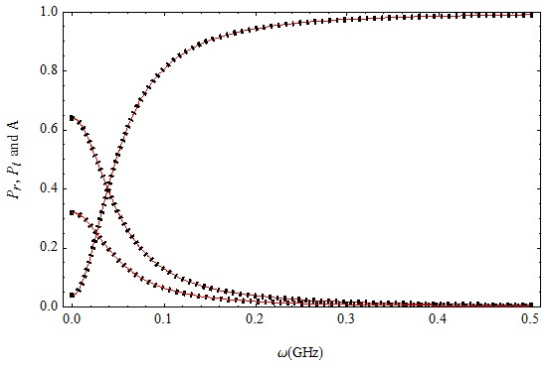


**Figure 2.** Comparison of (a) reflected power (b) transmitted power, and (c) absorbed power in the graphene-covered uniaxial crystal slab versus operating frequency for our case (solid line) and for Lenker [26] (dashed line).

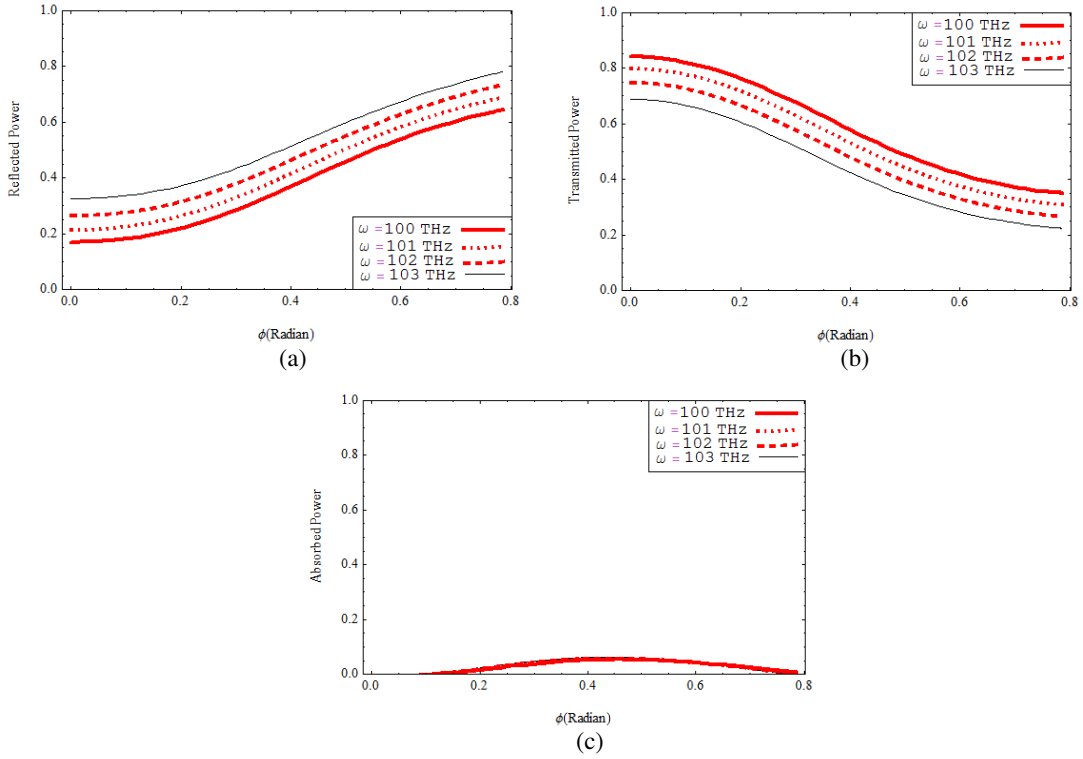


**Figure 3.** Comparison of (a) reflected (b) transmitted and (c) absorbed powers in the graphene-covered uniaxial crystal slab versus optical angle $\varphi$ for different values of $\omega$ for (case-i).

media separated by a graphene sheet derived by Stauber et al. in [18] and are left for readers. These comparisons confirm the validity and accuracy of the developed formulations of this work.

Three different cases of the constitutive parameters for the uniaxial anisotropic medium; $\varepsilon_t > 0$, $\varepsilon_z > 0$ (case-i), $\varepsilon_t < 0$, $\varepsilon_z < 0$ (case-ii), and $\varepsilon_t < 0$, $\varepsilon_z > 0$ (case-iii) are considered to illustrate the reflected power, transmitted power, and power absorption in the graphene-coated material. It is assumed that $\mu_t = \mu_z = \mu_0$ throughout the presented study. Figures 3(a)–(c) show the reflected powers, transmitted powers, and power absorption as functions of the optical angle $\varphi$ for case-i with $\omega = 100$ THz (thick solid line), $\omega = 102$ THz (dotted line), $\omega = 104$ THz (dashed line), and $\omega = 103$ THz (solid line) at $\Gamma = 2.6$ meV, $\varepsilon_t = 4\varepsilon_0$, $\varepsilon_z = 0.5\varepsilon_0$, and $\gamma = 0.96$. It is noted that at lower values of the incoming wave frequency, the reflected powers increase, and transmitted powers decrease. The same absorption powers appear to some extent along optical angle $\varphi$. The reflected and transmitted powers are inverse with the increase in the optical angle $\varphi$. It is also seen that there is no change in bandwidth of reflected and transmitted powers with variation in optical angle $\varphi$. Figures 4(a)–(c) show the reflected powers, transmitted powers and power absorption as functions of the optical angle $\varphi$ for case-ii with $\omega = 100$ THz (thick solid line), $\omega = 102$ THz (dotted line), $\omega = 104$ THz (dashed line), and $\omega = 103$ THz (solid line) at $\Gamma = 2.6$ meV, $\varepsilon_t = 4\varepsilon_0$, $\varepsilon_z = -0.5\varepsilon_0$, and $\gamma = 0.96$. It is noted that trends of the reflected power transmitted power and power absorption are the same as case-i with observation that both powers increase and decrease fast as compared to case-i along optical angle $\varphi$. Minute increase in absorption powers is observed. It is also seen that the bandwidths of reflected and transmitted powers decrease at higher value of optical angle $\varphi$ with these frequencies. Figures 5(a)–(c) show the reflected powers, transmitted powers and power absorption as functions of the optical angle $\varphi$ for case-iii with $\omega = 100$ THz (solid line), $\omega = 102$ THz (dotted line), $\omega = 104$ THz (dashed line), and $\omega = 103$ THz (solid line) at $\Gamma = 2.6$ meV, $\varepsilon_t = -4\varepsilon_0$, $\varepsilon_z = 0.5\varepsilon_0$, and $\gamma = 0.96$. It is noted that maximum constant power is reflected whereas no transmitted power and power absorption are observed.

Figures 6(a)–(c) depict the reflected powers, transmitted powers and absorbed powers for different thicknesses as varying with the optical angle $\varphi$ for ($\varepsilon_t > 0$, $\varepsilon_z > 0$) case i with $d = 10\,\mu$m (thick solid

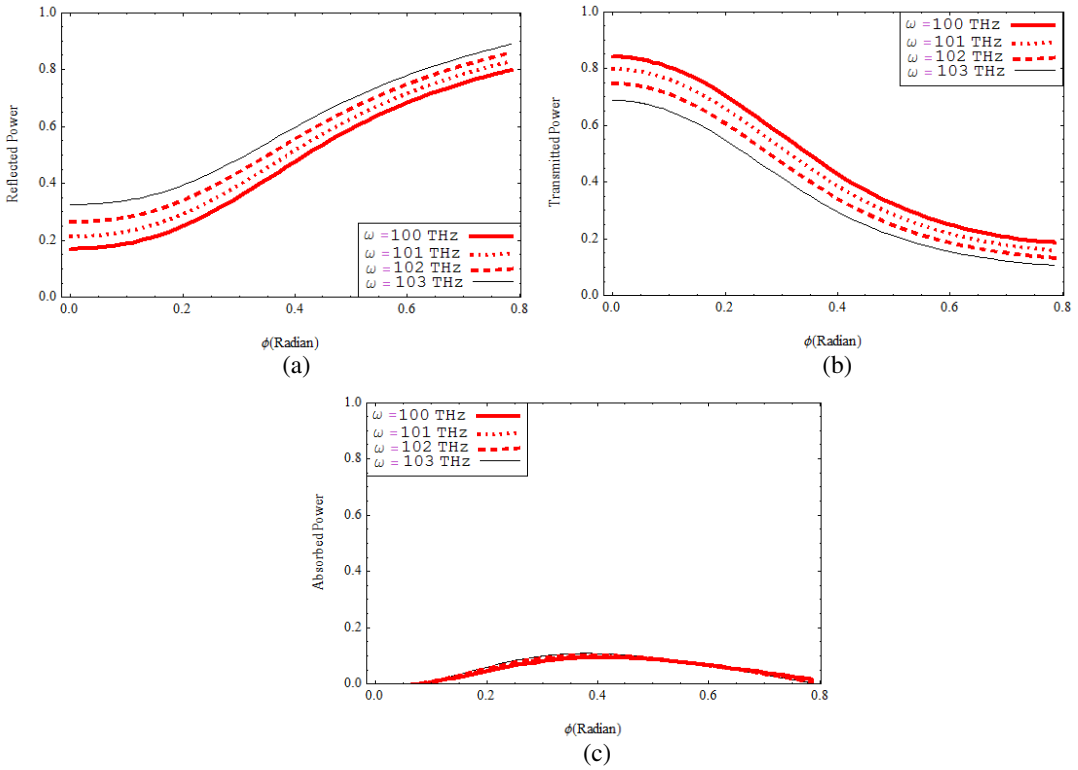


**Figure 4.** Comparison of (a) reflected (b) transmitted and (c) absorbed powers in the graphene-covered uniaxial crystal slab versus optical angle $\varphi$ for different values of $\omega$ case ii.

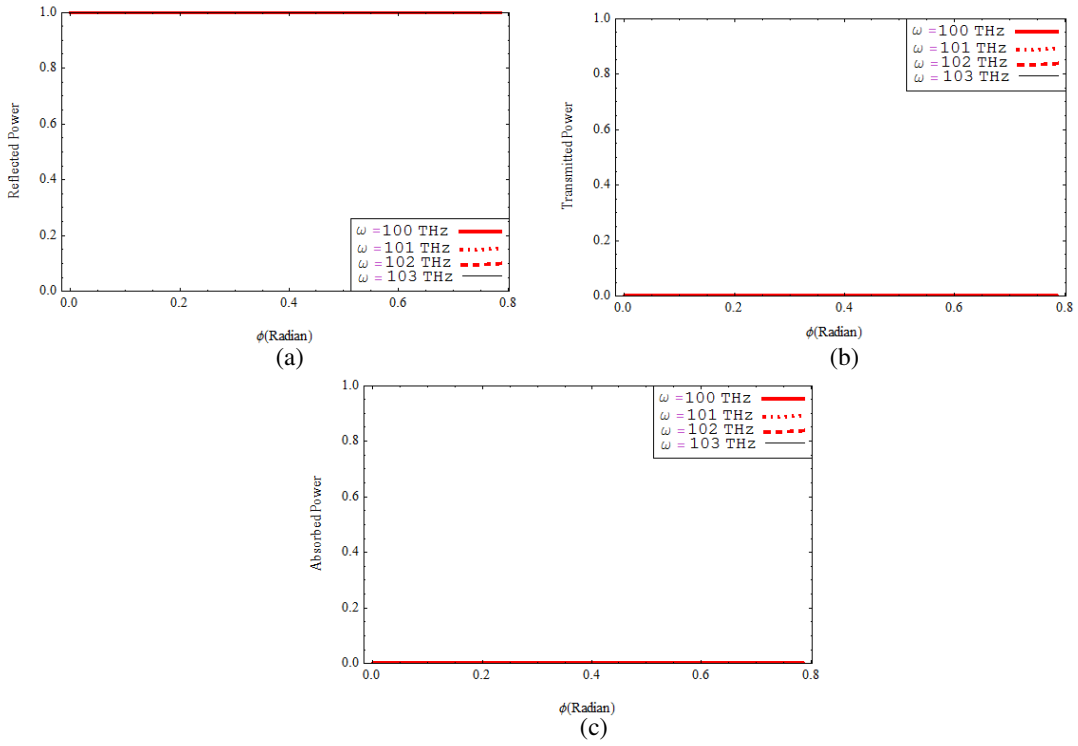


**Figure 5.** Comparison of (a) reflected (b) transmitted and (c) absorbed powers in the graphene-covered uniaxial crystal slab versus optical angle $\varphi$ for different values of $\omega$ case iii.

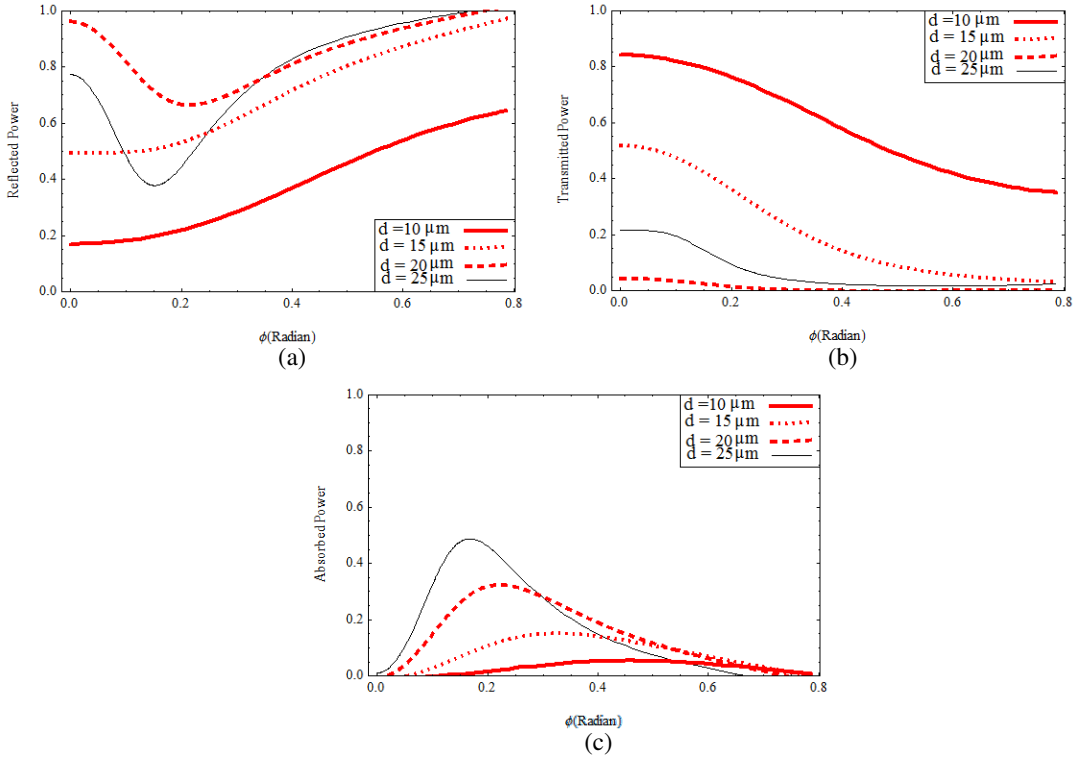


**Figure 6.** Comparison of (a) reflected (b) transmitted and (c) absorbed powers in the graphene-covered uniaxial crystal slab versus the optical angle $\varphi$ for different values of thickness of slab.

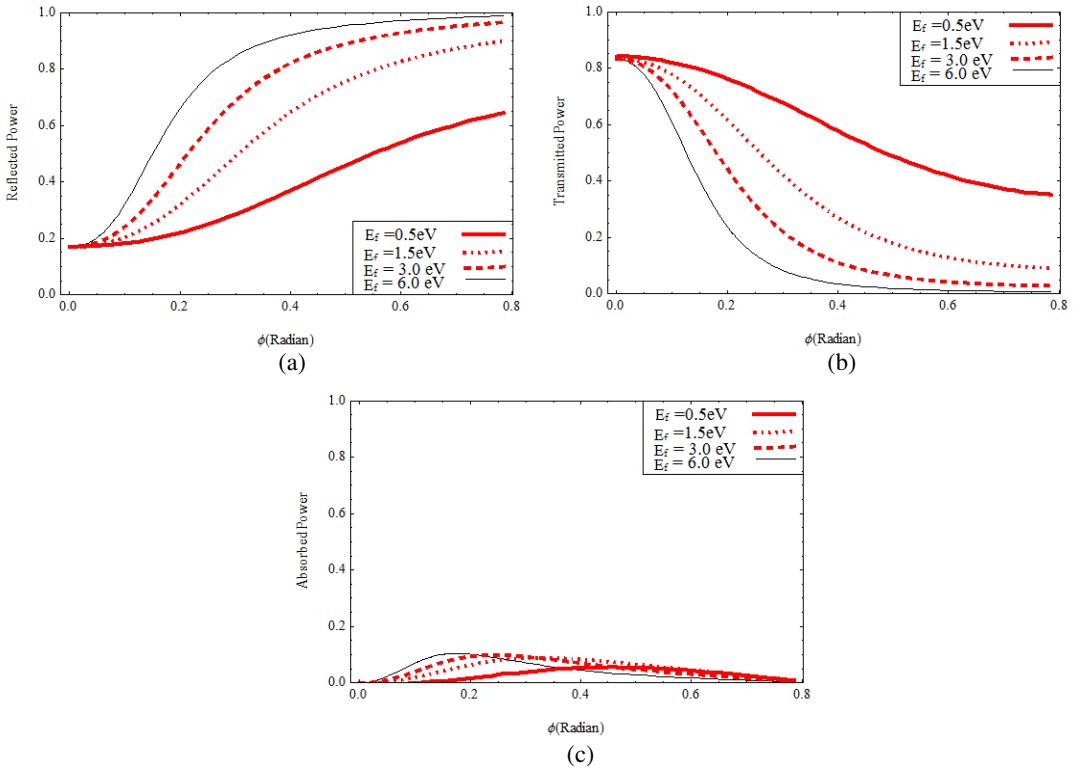


**Figure 7.** Comparison of (a) reflected (b) transmitted and (c) absorbed powers in the graphene-covered uniaxial crystal slab versus the optical angle $\varphi$ for different values of $E_F$.

line) $d = 15\,\mu\text{m}$ (dotted line), $d = 20\,\mu\text{m}$ (dashed line), and $d = 25\,\mu\text{m}$ (solid line) at $\Gamma = 2.6\,\text{meV}$, $\varepsilon_t = 4\varepsilon_0$, $\varepsilon_z = 0.5\varepsilon_0$, and $\gamma = 0.96$. It is observed that if the thickness of the slab is increased, then the reflected powers decrease, and transmitted powers increase with variation to optical angle $\varphi$. It is also observed that absorbed power increases with lower thickness of slab at lower value of optical angles. This feature might also provide an effective route for tuning the reflected powers, transmitted powers and absorbed powers.

Figures 7(a)–(c) show the reflected powers, transmitted powers, and absorbed powers as functions of the optical angle $\varphi$ for ($\varepsilon_t > 0$, $\varepsilon_z > 0$) case-i with Fermi energies $E_F = 0.5\,\text{eV}$ (thick solid line), $E_F = 1.5\,\text{eV}$ (dotted line), $E_F = 3.0e$ (dashed line), and $E_F = 6.0\,\text{eV}$ (solid line) at $\Gamma = 2.6\,\text{meV}$, $\varepsilon_t = 4\varepsilon_0$, $\varepsilon_z = 0.5\varepsilon_0$, and $\gamma = 0.96$. The reflected power increases, and the transmitted power decreases as the optical angle $\varphi$ increases. Lower values of Fermi level surges the rate of increase of reflected power and the rate of decrease of transmitted power with the optical angle $\varphi$. It is also noted that the reflectance and absorption can be maximized at higher values of Fermi level position at lower optical angle. It is observed that we can obtain reflected power further when increasing the Fermi energy more by means of decrease in conductivity of graphene. From obtained analysis it is shown that the external applied voltage plays a significant role in achieving the reflected power near the resonant frequency. The study offers an effective route of manipulating the powers by an external control field with such a configuration.

## 4. CONCLUSION

This paper has theoretically investigated the interaction of electromagnetic waves with a uniaxial crystal slab bounded by two graphene layers from both sides placed in free space. Formulations of the reflectance, transmittance, and absorption of a plane wave incident on the uniaxial crystal slab covered by the graphene sheets from both sides have been derived. It is displayed that higher reflectance and lower transmittance occur at lower frequencies of the incident wave for different positive and negative crystal material parameters. More importantly, the powers could be dynamically tuned with varying the thickness of the slab and the Fermi energy of the graphene. Moreover, it can be pointed out that the total reflectance can be attained with neither transmittance nor absorption if transverse permittivity of the crystal is negative. Finally, the reflected power and absorbed power are enhanced at higher values of the Fermi energy of graphene as expected. Such material scheme and analysis could have potential applications for the design of novel optical devices.

## ACKNOWLEDGMENT

The authors would like to extend their sincere appreciation to the Deanship of Scientific Research (DSR) at King Saud University for its funding of this research through the Research Group Project No. RG-1438-001.

## REFERENCES

1. Gusynin, V., S. Sharapov, and J. Carbotte, "Anomalous absorption line in the magneto-optical response of graphene," *Physical Review Letters*, Vol. 98, 157402, 2007.
2. Koppens, F. H., D. E. Chang, and F. J. Garcia de Abajo, "Graphene plasmonics: A platform for strong light–matter interactions," *Nano Letters*, Vol. 11, 3370–3377, 2011.
3. Nair, R., P. Blake, A. Grigorenko, K. Novoselov, T. Booth, T. Stauber, N. Peres, and A. Geim, "Fine structure constant defines visual transparency of graphene," *Science*, Vol. 320, 1308–1308, 2008.
4. Li, Y., F. Kong, and K. Li, "Graphene-based infrared lens with tunable focal length," *Progress In Electromagnetics Research*, Vol. 155, 19–26, 2016.
5. Mikhailov, S. and K. Ziegler, "New electromagnetic mode in graphene," *Physical Review Letters*, Vol. 99, 016803, 2007.

6. Ziegler, K., "Robust transport properties in graphene," *Physical Review Letters*, Vol. 97, 266802, 2006.
7. Correas-Serrano, D., J. S. Gomez-Diaz, J. Perruisseau-Carrier, and A. Alvarez-Melcon, "Graphene-based plasmonic tunable low-pass filters in the terahertz band," *IEEE Transactions on Nanotechnology*, Vol. 13, 1145–1153, 2014.
8. Abbas, F., A. Lakhtakia, Q. A. Naqvi, and M. Faryad, "An optical-sensing modality that exploits Dyakonov-Tamm waves," *Photonics Research*, Vol. 3, 5–8, 2015.
9. Wu, Y., M. Qu, Y. Liu, and Z. Ghassemlooy, "A broadband graphene-based THz coupler with wide-range tunable power-dividing ratios," *Plasmonics*, Vol. 12, 1487–1492, 2017.
10. Kong, M., Y. Wu, Z. Zhuang, W. Wang, and Y. Liu, "Graphene-based THz tunable bandstop filter with constant absolute bandwidth," *Progress In Electromagnetics Research Letters*, Vol. 71, 141–147, 2017.
11. Wu, H.-Q., C.-Y. Linghu, H.-M. Lu, and H. Qian, "Graphene applications in electronic and optoelectronic devices and circuits," *Chinese Physics B*, Vol. 22, 098106, 2013.
12. Dash, G., S. R. Pattanaik, and S. Behera, "Graphene for electron devices: The panorama of a decade," *IEEE Journal of the Electron Devices Society*, Vol. 2, No. 5, 77–104, 2014.
13. Kusmartsev, F., W. Wu, M. Pierpoint, and K. Yung, "Application of graphene within optoelectronic devices and transistors," *Applied Spectroscopy and the Science of Nanomaterials*, 191–221, Springer, 2015.
14. Kuila, T., S. Bose, P. Khanra, A. K. Mishra, N. H. Kim, and J. H. Lee, "Recent advances in graphene-based biosensors," *Biosensors and Bioelectronics*, Vol. 26, 4637–4648, 2011.
15. Madani, A., S. Zhong, H. Tajalli, S. Roshan Entezar, A. Namdar, and Y. Ma, "Tunable metamaterials made of graphene-liquid crystal multilayers," *Progress In Electromagnetics Research*, Vol. 143, 545–558, 2013.
16. Peres, N. and E. V. Castro, "Algebraic solution of a graphene layer in transverse electric and perpendicular magnetic fields," *Journal of Physics: Condensed Matter*, Vol. 19, 406231, 2007.
17. Kuzmin, D. A., I. V. Bychkov, and V. G. Shavrov, "Influence of graphene coating on speckle-pattern rotation of light in gyrotropic optical fiber," *Optics Letters*, Vol. 40, 890–893, 2015.
18. Stauber, T., N. Peres, and A. Geim, "Optical conductivity of graphene in the visible region of the spectrum," *Physical Review B*, Vol. 78, 085432, 2008.
19. Wang, G., Z. Gao, G. Wan, S. Lin, P. Yang, and Y. Qin, "Supported high-density magnetic nanoparticles on graphene by atomic layer deposition used as efficient synergistic microwave absorbers," 2014, DOI: 10.1007/s12274-014-0432-0.
20. Bao, Q., H. Zhang, B. Wang, Z. Ni, C. H. Y. X. Lim, Y. Wang, D. Y. Tang, and K. P. Loh, "Broadband graphene polarizer," *Nature photonics*, Vol. 5, 411–415, 2011.
21. Nilsson, J., A. C. Neto, F. Guinea, and N. Peres, "Transmission through a biased graphene bilayer barrier," *Physical Review B*, Vol. 76, 165416, 2007.
22. Jiang, L., Y. Xiang, X. Dai, and S. Wen, "Superluminal pulse reflection from graphene covered lossless dielectric slab," *IEEE Journal of Quantum Electronics*, Vol. 51, No. 3, 7000106, 2015.
23. Othman, M. A., C. Guclu, and F. Capolino, "Graphene-based tunable hyperbolic metamaterials and enhanced near-field absorption," *Optics express*, Vol. 21, 7614–7632, 2013.
24. Arrazola, I., R. Hillenbrand, and A. Y. Nikitin, "Plasmons in graphene on uniaxial substrates," *Applied Physics Letters*, Vol. 104, 011111, 2014.
25. Nikolaenko, A. E., N. Papasimakis, E. Atmatzakis, Z. Luo, Z. X. Shen, F. De Angelis, S. A. Boden, E. Di Fabrizio, and N. I. Zheludev, "Nonlinear graphene metamaterial," *Applied Physics Letters*, Vol. 100, 181109, 2012.
26. Lekner, J., "Normal-incidence reflection and transmission by uniaxial crystals and crystal plates," *Journal of Physics: Condensed Matter*, Vol. 4, 1387, 1992.